Radiation Pressure Instability Driven Eruptions in Low Mass X-ray Binary Disks

Eleanor Gentry

November 16, 2021

1 Introduction

Low-mass X-ray binary (LMXB) systems comprise a compact object (a neutron star or stellar-mass black hole), a main sequence star and an accretion disk. The accretion disk forms as the more compact object's gravity pulls mass from the secondary star (see Figure 1). Some LMXB accretion disks go through cycles of eruptions in which the luminosity increases rapidly. This project analyzes these eruptions numerically to study the mechanisms that cause and affect the eruptions, and uses that analysis to explain observational phenomena in LMXBs.

In the following, we first review the observational back ground for this project (Section 2). Next, we discuss the fundamentals of accretion theory (Section 3) and the specific instabilities thought to be in our system (Section 4). We then discuss the framework of our specific model as well as the nu merical methods used (Section 5). Finally, we present results from a series of simulations (Section 6) and the conclusions made from those results (Section 7).

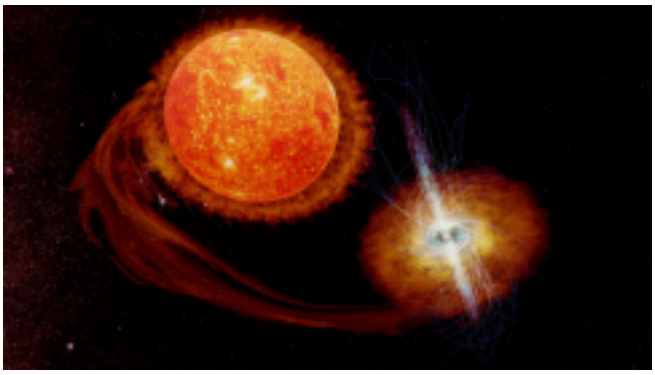

Figure 1: An artistic rendition of a low mass X-ray binary system. Artwork from Salvatore Orlando.

2 Observational Background

Low mass X-ray binaries are among the brightest X-ray ob jects in the sky. Some LMXBs undergo dramatic variability events ("eruptions") over time. We will focus on this subclass of transient LMXBs. During an eruption, the luminosity of the accretion disk suddenly increases and stays very high for a few weeks. In quiescence, the period between eruptions, the luminosity of these objects is very low, often unobservable.

Eruptions in LMXBs typically last from weeks to months, while quiescence lasts from months to years (see Figure 2). The luminosity of the disk is given in fraction of the Edding ton luminosity, the highest possible luminosity a spherically emitting gas can have before radiation pressure overcomes gravity. Expressing the luminosity in these units shows how effectively the disk radiates relative to its mass. The Edding ton luminosity is given by:

$$L_{\text{edd}} = 4\pi G M m_p c \sigma_T, \quad (1)$$

where G is Newton's gravitational constant, M is the mass of the central object, m_p is the mass of a proton, c is the speed of light in a vacuum and σ_T is the Thomson cross section (Frank et al., 2002). We see from Figure 2 that the luminosity of the disk is $< 2\times10^{-3}\ L/L_{\text{edd}}$ during quiescence and about 2×10^{-3} to 0.08 L/L_{edd} during an eruption.

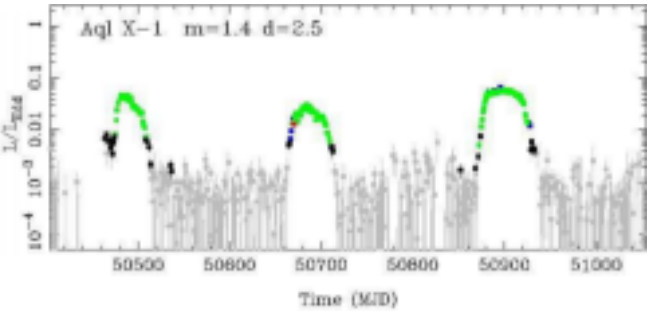

Figure 2: This figure shows the luminosity of a typical LMXB (Aql X-1) over time, i.e. a light curve. The x-axis is time in Modified Julian Days, and the y-axis is the observed luminos ity normalized by the Eddington luminosity. The green and black dots at higher luminosities show observed eruptions, and the gray lines at lower luminosities are detection limits, where the telescope cannot observe activity in the system, likely showing quiescence. Figure adapted from Done et al. (2007).

Notably, as an LMXB disk's luminosity changes, its spec trum also varies dramatically. The disk switches between a hard spectrum, dominated by high frequency X-rays (2.4×10^{18} Hz - 4.8×10^{18} Hz), and a soft spectrum, dominated by low frequency X-rays (4.8×10^{17} Hz - 1.5×10^{18} Hz), as shown in Figure 3. The soft state is typically interpreted as emission coming from a geometrically thin, radiatively effi cient accretion disk, radiating energy as a blackbody with a temperature of $T \approx 10^7$ K. The hard state is typically inter preted as emission from a radiatively inefficient, optically thin

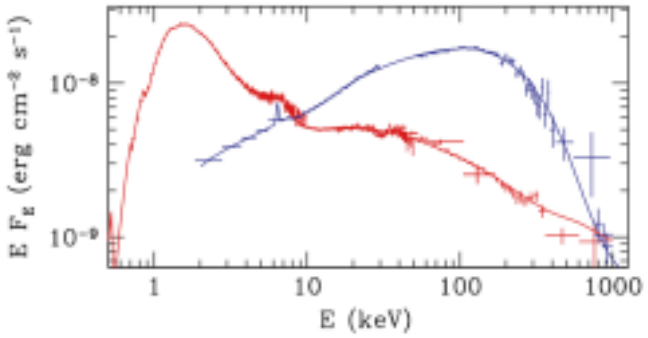

Figure 3: This figure shows the spectral states of Cygnus X 1. The blue line represents the hard state, and the red line represents the soft state. Figure from Done et al. (2007).

plasma with a temperature of $T \approx 10^9$ K. The hot plasma in the hard state is generally thought to be a hot accretion disk or a hot corona sandwiching a colder accretion disk or even the base of a magnetized jet (Markoff et al., 2001; Zdziarski and Gierli´nski, 2004; Yuan and Narayan, 2014; Kinch et al., 2021; Dexter et al., 2021).

The luminosity and the hardness ratio in the disk are strongly correlated (Remillard and McClintock, 2006). The hardness ratio is defined as the ratio of hard to soft X-rays at any given time. During an eruption, the observed hardness ratio follows a q-shape as a function of the observed luminos ity of the accretion disk as shown in Figure 4. When the disk rises to an eruption, it is in the hard state (blue). When the disk moves from an eruption to quiescence, it is in the soft state (green). For a given luminosity in the disk, the X-rays could be in two different hardness states. This (yet to be ex plained) hysteresis cycle implies that variables other than the accretion rate affect the disk's dynamics.

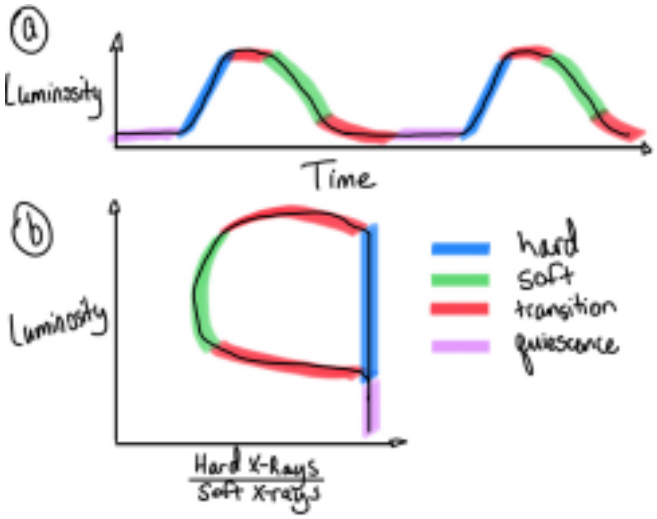

Figure 4: Here, the top panel shows the luminosity as a func tion of time (not to scale) which is how intensely the disk is radiating over time. The bottom panel shows the luminosity as a function of the hardness ratio, called a q-diagram (not to scale), or how intensely the disk is radiating at what fre quencies. On the light curve and the q-diagram, the colors show the respective spectral states, with red being the hard quiescent state, blue being the hard state during an eruption on the right side of panel b and the soft state of an eruption on the left side of panel b, green being the spectral transitions and purple being the return to quiescence. Different parts of the light curve correspond to each section of the q-diagram, which can show the relationship between the hardness ratio and the luminosity over time.

3 Accretion Theory

3.1 What is Accretion?

By observing the light emitted from an LMXB system, we can learn about what is happening in the accretion disk and ultimately understand the processes that drive accretion. Ac cretion is the accumulation of matter onto a central object. When accreted, an object will lose its gravitational potential energy and convert some of that energy into radiation. This change in gravitational potential is given by the equation:

$$\Delta E_{\text{acc}} = \frac{GMm}{R_*} \quad (2)$$

where m is the mass that is being pulled toward the central object and R_* is the radius of the central object. This equa tion tells us that if the central object has a higher mass or a smaller radius, more energy is released by accretion. The combination M/R_* explains why accreting black holes and neutron stars, with their very small radii, are so efficient at emitting light.

However, accretion is not trivial since the angular momen tum from the companion star's matter will prevent accretion. To understand this difficulty, consider the two typical forces acting on an object orbiting a central mass. The first, grav ity, pulls the object towards the central object. The second, the centrifugal force, pushes the matter away from the cen tral object. The balance of gravity and centripetal forces will keep the matter in orbit at the Keplerian frequency at a given radius R, defined as

$$\Omega = \sqrt{\frac{GM}{R^3}}, \quad (3)$$

unless another force is introduced to change that equilibrium. In order to actually accrete matter, angular momentum must be transported out of the disk, which requires a torque to act on the disk. A natural way of producing a torque on the disk is through the friction between two consecutive an nuli of the accretion disk. Because the annulus at the outer radius moves slower than the annulus at the inner radius, as can be seen in Equation 3, the outer annulus slows the inner radius down, which transports angular momentum away from the inner annulus. This mechanism of angular momentum is called viscous transport.

3.2 The Thin Disk Model

The thin disk model is a standard theoretical model of accre tion disks that assumes an axisymmetric, vertically-averaged disk rotating at the Keplerian frequency

(Shakura and Sun yaev, 1973). The disk is geometrically thin, i.e. the height H of the disk is much less than the radius R of the disk. The small height justifies using a vertically-averaged model. Such a thin disk is very dense and radiates efficiently. The thin disk model is a good representation of the soft state of a LMXB.

Traditionally, the thin disk model assumes that angular mo mentum is transported by viscous internal torques in the disk, causing radial drift inward. However, the molecular viscosity in an accretion disk is orders of magnitude too low to explain the evolution of any accreting systems. Instead, the thin disk model relies on an “effective” viscosity due to turbulence and other unknown effects. In the thin disk model, the effective viscosity is parameterized as

$$\nu = \alpha C_s H. \quad (4)$$

where C_s is the sound speed, H is the height of the disk and α is a free parameter of the model, which is estimated to be between 0 and . 1 (Shakura and Sunyaev, 1973).

An alternative form of the thin disk model assumes that an gular momentum is transported through magnetized winds, which eject matter and angular momentum from the disk (Blandford and Payne, 1982) thus inducing accretion in the disk. Simulations show that wind-driven angular momen tum transport dominates at high magnetization while viscous driven angular momentum transport dominates at low mag netization.

3.3 Evolution Timescales in the Disk

In this section, we will characterize the timescales of different processes operating in the disk.

The shortest timescale is the orbital timescale, which is how fast the matter in the disk orbits the central object. This timescale is given by the equation

$$t_{\rm orb} \equiv \frac{1}{\Omega} = \sqrt{\frac{R^3}{GM}} \quad (5)$$

The inner disk will evolve much faster than the outer disk due to this dependence on R. For an LMXB system with a central mass of 5 $M_\odot$, the typical inner radius of 10^6cm has an orbital timescale (period) of about 4×10^{-5}s. At a typical outer radius of 10^{11} cm, the orbital timescale will be about 1300 seconds, or about 22 minutes. Because eruptions happen over weeks, the orbital timescale is much faster than the duration of an eruption everywhere in the disk.

The viscous timescale shows how fast accretion will happen as a result of viscous torques in the disk (Frank et al., 2002). This timescale is given by the equation

$$t_{\rm visc} = \frac{R}{v_R} = \frac{1}{\alpha}\left(\frac{H}{R}\right)^{-2} t_{\rm orb}. \quad (6)$$

For typical values of $\alpha = 0.1$ and $H/R = 0.01$, the viscous timescale is about 4 seconds at the disk inner radius, com pared to about 50 months at the outer radius. The viscous time at the outer radius is comparable to the time in between eruptions.

The thermal timescale shows how fast the temperature will return to equilibrium in the disk. This timescale is given by the equations

This timescale is about 4×10^{-4}seconds at the inner radius of a typical LMXB, and about 1.3×10^4seconds, or about 4 hours at the outer radius of a typical LMXB. The thermal timescale is the typical timescale on which the disk rises to its maximum temperature during an eruption and on which the disk cools down to quiescence at the end of an eruption.

Taken together, these simple estimates already tell us that the durations of the eruption and of quiescence are linked to changes in the density of the disk, whereas the duration of the rise to outburst and decline to quiescence are linked to changes in the temperature of the disk.

4 Temporal evolution of accretion disks

In this section, we will describe two thermal instabilities that can suddenly change the temperature in the disk and cause the observed eruptions: the ionization instability (Section 4.1) and the radiation pressure instability (Section 4.2).

A disk can have both stable and unstable thermal equi libria, which cause both eruptions and the steady states in between those eruptions. Figure 5 and Figure 6 each show an “S-curve” where each point represents the thermal equi librium of the disk at a given radius and a given α. The temperature as a function of the density in the disk has a characteristic “s” shape due to the sudden heating and cool ing in the disk caused by instabilities. The upper and lower branches of each “s” are at a stable equilibrium, i.e. small deviations from that temperature will immediately return to the temperature represented on the plot. The middle branch is an unstable equilibrium. When there is a deviation from the equilibrium temperature in this regime, the temperature will continue to change at an increasing rate. This rapid tem perature change will only stop when the temperature in the disk reaches another point of equilibrium, on either the top or bottom branch of the s-curve.

Here, we will describe two types of instabilities thought to cause eruptions in LMXBs: the hydrogen ionization in stability (Section 4.1) and the radiation pressure instability (Section 4.2).

4.1 Hydrogen Ionization Instability

The hydrogen ionization instability is caused by hydrogen in the disk ionizing suddenly at about 10^4 K. The sudden ion ization causes the heating rate in the disk to increase much more than the cooling rate. During quiescence, the disk’s temperature and density are on the bottom branch of the s curve, here called the cold branch (Figure 5). On the cold branch, none of the hydrogen is ionized. Mass accumulates in a ring at any given radius R because the inflow rate from the secondary star $\dot{M}_{\rm in}$ is bigger than the accretion rate onto the central object $\dot{M}$, moving the ring to the right and up along the s-curve. Eventually the temperature will reach 10^4 K, causing all of the hydrogen in the disk to ionize. As a result, the temperature increases rapidly, taking the disk di

$t_{th} = \frac{H}{R}\frac{R}{2}$

$t_{visc} = \frac{1}{\alpha} t_{orb}$. (7)

rectly from the bottom branch to the top branch of the “s” shape. The top branch is here called the warm branch. Be cause $\dot{M}_{in}$, the local mass accretion rate is now larger than 3

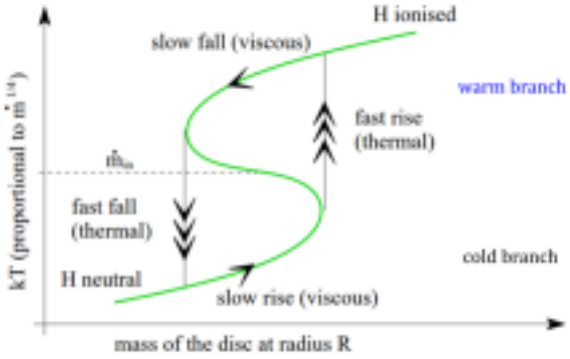

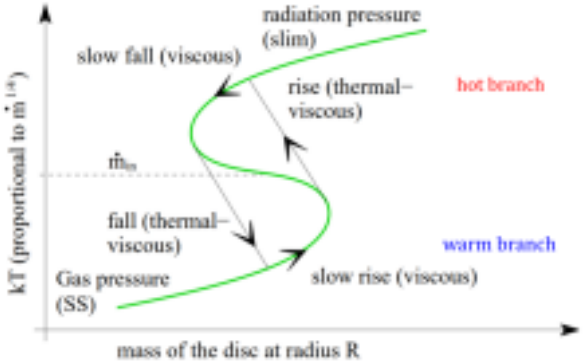

Figure 5: This figure shows an s curve, with mass of the disk at a given radius on the x-axis, and the temperature on the y-axis, in the hydrogen ionization instability range, which is around 10^4 K. (Done et al., 2007)

Figure 6: The x axis of this figure is the mass of the disk at a given radius, and the y-axis is the temperature of the disk in the radiation pressure instability range, which is around 10^8 K. This figure shows only the temperature range where hydro gen is always ionized, so the hydrogen ionization instability (shown in Figure 5) is not present. Figure adapted from Done et al. (2007).

the ring will start to decrease in mass. Since the disk stays in equilibrium, the decrease in mass also means a decrease in temperature. Once the temperature returns to 10^4 K, the hydrogen will recombine, and the temperature in the disk will suddenly drop back to the cold branch (H¯oshi, 1979).

The eruptions in an LMXB system are thought to be trig gered by the hydrogen ionization instability (Dubus et al., 2001). However, this type of instability alone does not ex plain the hysteresis observed in the q-diagram in Figure 4.

4.2 Radiation Pressure Instability

The radiation pressure instability could also be present in the high-temperature portion of an LMXB disk. Though it is not clear how this instability manifests observationally, it could cause eruptions mostly at the inner disk when the disk has a high temperature and low density.

There are two conditions to be unstable to the radiation pressure instability:

1. The disk must radiate through Compton scattering, not free-free emission.

2. Radiation pressure must dominate gas pressure.

The first condition arises because the cooling rate is much less temperature dependent when Compton scattering domi nates. This way, the disk will cool slower as the temperature increases rapidly to an eruption. The second condition re flects the change in heating rate between the gas pressure dominated and the radiation pressure-dominated regimes. When gas pressure dominates in the disk, the disk heats at a rate proportional to the temperature. On the other hand, when radiation pressure dominates in the disk, the disk heats at a rate proportional to T^4. This heating rate is much faster than the disk can cool, and will cause a sudden increase in temperature.

During quiescence, the disk is on the bottom branch of the s-curve, where gas pressure dominates over radiation pressure (Figure 6). The bottom branch in this figure is the top branch of the hydrogen ionization instability (top branch in Figure 5), which is the warm branch. As mass accumulates in the disk and the temperature rises, the disk will reach a critical temperature in which the heating rate will go as T^4instead of T, so the temperature will rapidly increase, and the disk will be on the top branch, here called the hot branch. As the matter in the disk accretes onto the central object, the temperature and mass of the disk will both decrease until the temperature returns to the same critical point when the heating rate will go back to being proportional to T, not T^4, because the radiation pressure is no longer dominating. At that time, the disk will return to the bottom branch of the s, which is the quiescent state (Taam and Lin, 1984).

5 Framework

5.1 Our Model

In our model, we consider an accretion disk composed of two sections, shown in Figure 7. The turbulent disk, where turbulent-driven angular momentum transport dominates, is located in the outer disk. This section of the disk is weakly magnetized. It is at a relatively lower temperature, so the hydrogen ionization instability drives eruptions in the turbu lent disk (Section 4.1). The majority of the disk is turbulent driven when the disk is in the soft state, or during an eruption.

The wind-driven disk, where magnetic winds dominate the angular momentum transport, is located in the inner disk. This section of the disk is highly magnetized. We will

assume that dissipation of magnetic energy in the magnetic winds produce the hard X-rays necessary to explain the hard state. With this assumption, it follows that the majority of the disk is wind-driven when the disk is in the hard state.

We aim to explain the dynamical behavior of LMXBs and the q-diagram by varying the transition radius between the in ner magnetized disk and the outer turbulent one. Our model, presented below, evolves radiation pressure, which is not in cluded in traditional thin disk models.

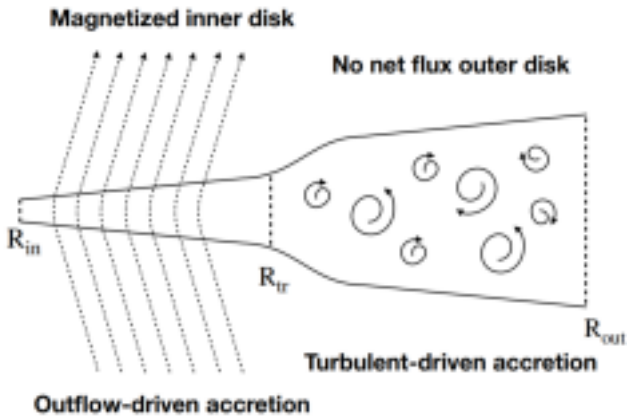

Figure 7: This schematic from Scepi et al. (2021) shows the two main sections of the disk, the inner, wind driven, highly magnetized section, and the outer, turbulent, weakly magne tized section.

5.2 Numerical Methods

The disk instability model (DIM, Hameury et al. (1998)) is often used to simulate LMXBs accretion disks (Dubus et al., 2001). The DIM is an axisymmetric and vertically averaged combination of the MHD equations. It solves the conservation of mass

$$\frac{\partial \Sigma}{\partial t} = \frac{1}{2\pi R}\frac{\partial \dot{M}}{\partial R}, \quad (8)$$

and the conservation of energy

$$\frac{\partial T}{\partial r} - (\Gamma - 1)\frac{T}{r}\partial_r(rv_r) = Q^+ - Q^- \frac{\partial t}{\Sigma} + v_r\frac{\partial T}{\partial r}$$

4

sure are defined respectively as

$$P_{gas} = \rho k_B T \frac{}{\mu m_p}, \quad (12)$$

$$P_{rad} = Q^- P_{mag} = B_z^2 \frac{4}{\tau_{tot} + 3}, \quad (13)$$

In these equation, ρ is the gas's mass density, $\tau_{tot} = \Sigma(\kappa_T + \kappa_{ff})$ with κ_T the electron scattering opacity and κ_{ff} the free free opacity, and B_z is the vertical magnetic field. In the simulations presented in Section 6, B_z has a fixed value and configuration and thus controls whether we have a turbulent driven disk or a wind-driven disk.

The heating rate Q^+ and cooling rate Q^- are given by Q^+

$$= \frac{9}{4}\alpha(\beta)\,\Omega^3 H^2 \Sigma \quad (15)$$

$$Q^- = 2\sigma T_{eff}^4 \frac{8\pi}{} \quad (14)$$

$$\frac{1}{3\tau_{tot} + \tau_?^2} \frac{-1}{1 + 4} \quad (16)$$

where the effective temperature T_{eff} is a function of Σ and T and is computed using the prescriptions from Latter and Pa paloizou (2012). The factor in parentheses in Eq. 16 bridges the regime of optically thin cooling and the regime of op tically thick cooling as in Esin et al. (1996). In addition, $\tau_? = 3\tau_{tot}\tau_a/2$ and $\tau_a = Q_{brem}/(\sigma T_{eff}^4)$ where Q_{brem} is the bremsstrahlung cooling rate of an optically thin plasma. In Eq. 16, σ is the Stefan-Boltzmann constant (not to be con fused with σ_T). These equations are solved numerically to simulate the time-dependent behavior of the disk on an eruption timescale.

$$\frac{2m_p}{5k_B\mu}. \quad (9)$$

6 Results

In these equations, Σ is the surface density, T is the temperature, v_r is the accretion speed, Γ is the adiabatic exponent (which depends on radiation pressure as expressed in Lasota and Pelat (1991)), k_B is Boltzmann constant, and μ is the mean molecular weight.

The accretion rate $\dot{M}$ evolves according to

$$\frac{\partial \dot{M}}{\partial R} = 4\pi R\Omega \left[\frac{3}{2R^2}\alpha(\beta)\,\Sigma\Omega^2 H^2 + q(\beta)\,B_z^2 R\Omega \right], \quad (10)$$

where α is the turbulent parameter quantifying the strength of the turbulent torque, q is the dimensionless number quantifying the strength of the wind-driven torque. The values of α and q both change with the magnetization of the disk according to prescriptions from Scepi et al. (2020). The prescriptions give wind-driven torques for a high magnetizations and turbulent-driven torques at low magnetization. The magnetization is quantified by the plasma β parameter as

$$\beta = \frac{P_{\rm gas} + P_{\rm rad}}{P_{\rm mag}}. \quad (11)$$

Higher values of β correspond to weaker disk magnetizations. Here, the gas pressure, radiation pressure and magnetic pres

Figure 8 shows the ratio of radiation pressure to gas pressure as a function of time for two turbulent-driven simulations with different $\dot{M}$. With an accretion rate of 10^{15} g/s, the ratio of radiation pressure to gas pressure stays about constant, showing that the disk is in a steady state (blue solid line). Because $P_{\rm rad}/P_{\rm gas} < 1$, the steady state is in the gas pressure dominated regime. If all other parameters remain the same, but the mass flux increases to 10^{16} g/s (dashed green line), the disk erupts in the radiation pressure dominated regime with the ratio of radiation to gas pressure oscillating between 2.2 and 0.1 on a timescale of a fraction of orbital time.

We compare all of the turbulent-driven simulations, with varied mass fluxes and radii, in Figure 9. The left column shows simulations of a disk extending from $10^6$to 10^7cm. At a lower accretion rate of 10^{15} g/s, we see a steady state on the warm branch. As the accretion rate increases to 10^{16} and 10^{17} g/s, the disk is unstable and has eruptions. These eruptions are in the thermal regime of radiation pressure instability, not hydrogen ionization instability. Then, as the accretion rate increases to 10^{18} g/s, the disk is in a stable regime again, this time on the hot branch.

The right column shows simulations of a disk extending from $10^7$to 10^8cm. At these larger radii, the disk stays on the warm branch for accretion rates of 10^{17} and 10^{18} g/s. Eruptions start to happen at 10^{18} g/s, a much higher accretion rate than at the smaller disk extent. At larger radii, the disk temperature at the same accretion rate is smaller. The temperature increases with accretion rate, so at a larger radius, a larger accretion rate is needed to reach a thermal regime that would instigate a radiation pressure instability driven eruption. This result is consistent with Eq. 2.17 of Shakura and Sunyaev (1973) that the boundary between a gas pressure dominated disk and a radiation pressure dominated disk happens at a radius R_{gr}, where

6.1 Local Simulations

In this work, we use the term "local" to describe a simulation of a limited radial section of the disk. The simulations described in this section show disks that extend from either 10^6 to 10^7cm or from $10^7$to 10^8cm. The disk's eruptions are highly sensitive to the accretion rate. To study this dependence, first we simulated the most inner part of the disk and artificially changed the accretion rate at the outer boundary. In a global simulation, this change in accretion rate would be driven by hydrogen ionization eruptions in the turbulent disk.

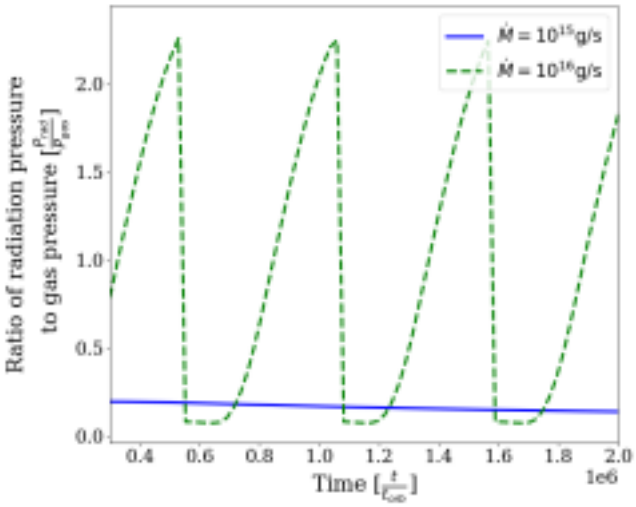

Figure 8: This figure shows the ratio of radiation pressure to gas pressure at a given radius r = 2.2 × 10^6cm. The blue solid line shows a steady state with an accretion rate of 10^{15} g/s, where gas pressure dominates the disk. The green dashed line shows eruptions, where the radiation pressure increases to dominate the disk. This simulation has an accretion rate of 10^{16} g/s.

$$R_{gr} \propto \dot{M}^{16}$$

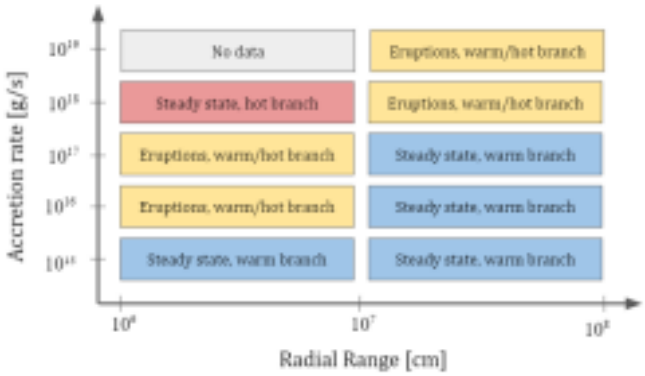

Figure 9: This schematic represents the parameters in which an entirely turbulent disk (with no wind-driven component) will be unstable and have eruptions. It is clear from the figure that as the radial range of the disk increases, the unstable accretion rate regime also increases.

higher accretion rate to get to the temperature-density regime that will cause an eruption.

Figure 9 and 10 give an idea of what to expect in the inner most parts of an accretion disk based on the behavior

$$(1 - R_{gr}^{-1/2})^{16} \propto \dot{M}^{21}. \quad (17)$$

In the next suite of simulations, we include both wind driven angular momentum transport and turbulent-driven an gular momentum transport (Figure 10). Though we find the same general trend with $\dot{M}$ as in Figure 9, there is a much more narrow regime for eruptions to occur in this type of disk. The eruptions occur only at an accretion rate of 10^{17} g/s, rather than at 10^{16} and 10^{17} g/s in the purely turbu lent case. This narrow range is because wind driven angular momentum transport cools disks very efficiently, so it takes a magnetized disks to observe the radiation pressure instabil ity. The higher accretion rate is needed because a strongly magnetized disk is colder than a weakly magnetized disk for a same accretion rate. Hence if the inner parts of LMXBs are strongly magnetized, LMXBs may never reach the regime where the radiation pressure instability dominates and the radiation pressure instability may not play a role in the hys teresis. This hypothesis should be explored using simulations of the full disk where the mass accretion rate and the mag netic field self-consistently change in the inner disk depending on the outcome of the ionization instability in the outer disk.

in the outer disk. Because eruptions in the outer part of the disk are likely to be driven by the hydrogen ionization instability, these results help us predict eruptions at the wind-driven part of the accretion disk.

7 Conclusions

LMXBs are binary systems with a compact object like a black hole or a neutron star at the center, and a secondary solar type star. The accretion disk between these two objects ac cretes matter from the secondary star onto the compact object through turbulent and wind driven processes. The disk will go through cycles of increased luminosity over time. During these cycles, the spectral state of LMXBs also changes follow ing a hysteresis cycle. This project investigates the role of the radiation pressure instability in the hysteresis of LMXBs.

To accurately study the evolution of the disk during the hysteresis cycle, we perform a series of 1D simulations evolv ing the radial structure of the disk over time for different mass accretion rates in the disk. In order to understand the role of the radiation pressure instability, which develop at small radii, we focus on simulating small parts of the inner disk. We study two types of disk: strongly magnetized disks and weakly magnetized disks. We find that for strongly magne tized disks, higher accretion rates are needed than for weakly

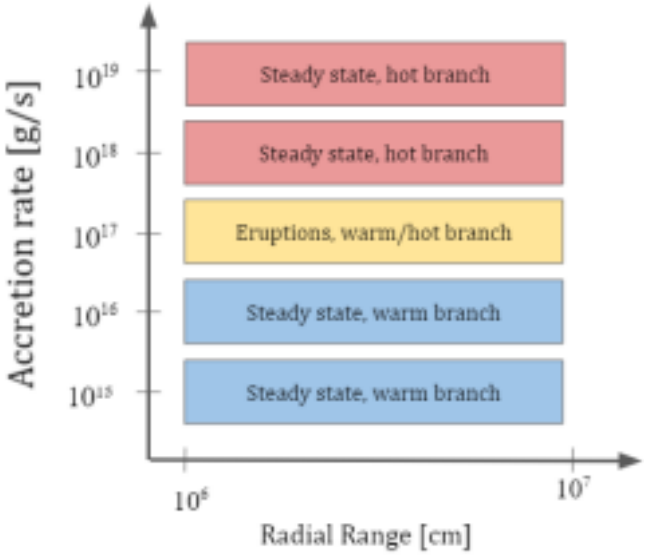

Figure 10: This schematic, similarly to Figure 9, shows which accretion rates give eruptions in a disk that has both a turbulent-driven and a wind-driven part of the disk.

8 Acknowledgments

The author thanks Jason Dexter, Nico Scepi, and Lia Hankla for their mentorship and collaboration on this project. This work utilized resources from the University of Col orado Boulder Research Computing Group, which is sup ported by the National Science Foundation (awards ACI 1532235 and ACI-1532236), the University of Colorado Boul der, and Colorado State University.

References

Juhan Frank, Andrew King, and Derek J. Raine. *Accretion Power in Astrophysics: Third Edition*. 2002.

Chris Done, Marek Gierli´nski, and Aya Kubota. Modelling the behaviour of accretion flows in X-ray binaries. Every thing you always wanted to know about accretion but were afraid to ask. A&A Rev., 15(1):1–66, December 2007. doi: 10.1007/s00159-007-0006-1.

S. Markoff, H. Falcke, and R. Fender. A jet model for the broadband spectrum of XTE J1118+480. Synchrotron emission from radio to X-rays in the Low/Hard spectral state. A&A, 372:L25–L28, June 2001. doi: 10.1051/ 0004-6361:20010420.

A. A. Zdziarski and M. Gierli´nski. Radiative Processes, Spec tral States and Variability of Black-Hole Binaries. *Progress of Theoretical Physics Supplement*, 155:99–119, January 2004. doi: 10.1143/PTPS.155.99.

Feng Yuan and Ramesh Narayan. Hot Accretion Flows Around Black Holes. ARA&A, 52:529–588, August 2014. doi: 10.1146/annurev-astro-082812-141003.

Brooks E. Kinch, Jeremy D. Schnittman, Scott C. Noble, 7 Timothy R. Kallman, and Julian H. Krolik. Spin and Accre tion Rate Dependence of Black Hole X-Ray Spectra. *arXiv e-prints*, art. arXiv:2105.09408, May 2021.

Jason Dexter, Nicolas Scepi, and Mitchell C. Begelman. Radi ation GRMHD Simulations of the Hard State of Black Hole X-Ray Binaries and the Collapse of a Hot Accretion Flow. ApJ, 919(2):L20, October 2021. doi: 10.3847/2041-8213/ ac2608.

Ronald A. Remillard and Jeffrey E. McClintock. X-Ray Properties of Black-Hole Binaries. ARA&A, 44(1):49–92, September 2006. doi: 10.1146/annurev.astro.44.051905. 092532.

N. I. Shakura and R. A. Sunyaev. Reprint of 1973A&A....24..337S. Black holes in binary systems. Ob servational appearance. A&A, 500:33–51, June 1973.

R. D. Blandford and D. G. Payne. Hydromagnetic flows from accretion disks and the production of radio jets. MNRAS, 199:883–903, June 1982. doi: 10.1093/mnras/199.4.883.

R. H¯oshi. Accretion Model for Outbursts of Dwarf Nova. *Progress of Theoretical Physics*, 61(5):1307–1319, May 1979. doi: 10.1143/PTP.61.1307.

G. Dubus, J. M. Hameury, and J. P. Lasota. The disc in stability model for X-ray transients: Evidence for trunca tion and irradiation. A&A, 373:251–271, July 2001. doi: 10.1051/0004-6361:20010632.

R. E. Taam and D. N. C. Lin. The evolution of the inner regions of viscous accretion disks surrounding neutron stars. ApJ, 287:761–768, December 1984. doi: 10.1086/162734.

Nicolas Scepi, Mitchell C. Begelman, and Jason Dexter. QPOs in compact binaries from small-scale eruptions in an inner magnetized disc. MNRAS, 500(1):1547–1556, Jan uary 2021. doi: 10.1093/mnras/staa3410.

Jean-Marie Hameury, Kristen Menou, Guillaume Dubus, Jean-Pierre Lasota, and Jean-Marc Hure. Accretion disc outbursts: a new version of an old model. MNRAS, 298(4): 1048–1060, August 1998. doi: 10.1046/j.1365-8711.1998. 01773.x.

J. P. Lasota and D. Pelat. Variability of accretion discs around compact objects. A&A, 249(2):574–580, September 1991.

N. Scepi, G. Lesur, G. Dubus, and J. Jacquemin-Ide. Mag netic field transport in compact binaries. A&A, 641:A133, September 2020. doi: 10.1051/0004-6361/202037903.

H. N. Latter and J. C. B. Papaloizou. Hysteresis and thermal limit cycles in MRI simulations of accretion discs. MNRAS, 426(2):1107–1120, October 2012. doi: 10.1111/j.1365-2966. 2012.21748.x.

Ann A. Esin, Ramesh Narayan, Eve Ostriker, and Insu Yi. Hot One-Temperature Accretion Flows around Black Holes. ApJ, 465:312, July 1996. doi: 10.1086/177421.